Contrib Mineral Petrol (2006) 151: 141–157
DOI 10.1007/s00410-005-0051-6

ORIGINAL PAPER

Robert W. Luth

Experimental study of the $CaMgSi_2O_6$–CO_2 system at 3–8 GPa

Received: 31 May 2005 / Accepted: 10 November 2005 / Published online: 16 December 2005

Abstract The melting relationships in the system $CaMgSi_2O_6$ (Di)–CO_2 have been studied in the 3–8 GPa pressure range to determine if there is an abrupt decrease in the temperature of the solidus accompanying the stabilization of carbonate as a subsolidus phase. Such a decrease has been observed previously in peridotitic and some eclogitic systems. In contrast, the solidus in the Di–CO_2 system was found to decrease in a gradual fashion from 3 to 8 GPa. This decrease accompanies an evolution in the composition of the melt at the solidus from silicate-rich with minor CO_2 at 3 GPa to carbonatitic at 5.5 GPa, where the carbonation reaction Diopside + CO_2 = Dolomite (Dol) + Coesite (Cst) intersects the solidus. The near-solidus melt remains carbonatitic at higher pressure, consistent with carbonate being the dominant contributor to the melt. Based on previous studies in both eclogitic and peridotitic systems, this conclusion can be extended to more complicated systems: once carbonate is a stable subsolidus phase, it plays a major role in controlling both the temperature of melting and the composition of the melt produced.

Introduction

A characteristic of the phase relationships in peridotite–CO_2 systems at high pressures and high temperatures is the pronounced decrease in solidus temperatures accompanying the appearance of carbonate as a stable mineral at the solidus. In the model system CaO–MgO–SiO_2–CO_2, where the relevant melting reaction involves olivine, orthopyroxene, and clinopyroxene, the solidus temperature decreases ~300°C at ~2.5 GPa, where dolomite becomes stable at the expense of CO_2 via the reaction forsterite (Fo) + diopside (Di) + CO_2 = enstatite (En) + dolomite (Dol) (White and Wyllie 1992 and references therein). This temperature decrease produces a "ledge" on the solidus (Fig. 1). This topology survives the addition of alumina to the system (Fig. 1). The nature of the melt changes concomitantly across this interval, from a basaltic silicate melt with some dissolved CO_2 at lower pressure to a carbonatitic melt with minimal silica. The presence or absence of carbonate in a peridotitic system therefore has profound implications for the temperature of the solidus, for the nature of the melt produced, and hence for the conditions where a CO_2-bearing melt or fluid would be stable in the mantle, as has been recognized since the 1970s (Eggler 1974, 1976, 1978; Wyllie and Huang 1975, 1976).

The other major lithology present in the mantle is eclogite of a generally basaltic bulk composition. Carbonation reactions appropriate for an eclogitic (clinopyroxene + garnet) mineral assemblage are at higher pressures than those for a peridotitic assemblage (Luth 1999). The intersection of these reactions with the appropriate solidus therefore would be at higher pressures and temperatures, which might make the increase in solubility of CO_2 in the liquid with increasing pressure play a larger role than in the peridotite systems. The offset might also allow a depth interval in the mantle where a CO_2-rich fluid is stable in eclogitic lithologies but carbonate is stable in peridotite. Given the current interest in carbonatitic fluids and melts as potential metasomatizing agents in the mantle, understanding the effect of CO_2 on melting relationships in eclogitic systems is necessary.

This study explores the topology of the melting and carbonation phase equilibria in the simple system, $CaMgSi_2O_6$–CO_2, to see if a solidus "ledge" is characteristic of silicate–CO_2 systems. It builds on earlier work on the melting phase relations in this system at pressures to 4 GPa by Eggler and Rosenhauer (1978), and on the study of the Dol + 2 Cst = Di + 2 CO_2 reaction by Luth (1995).

Communicated by: T. L. Grove

R. W. Luth (✉)
C.M. Scarfe Laboratory for Experimental Petrology,
Department of Earth and Atmospheric Sciences,
University of Alberta, T6G 2E3 Edmonton, AB, Canada
E-mail: robert.luth@ualberta.ca

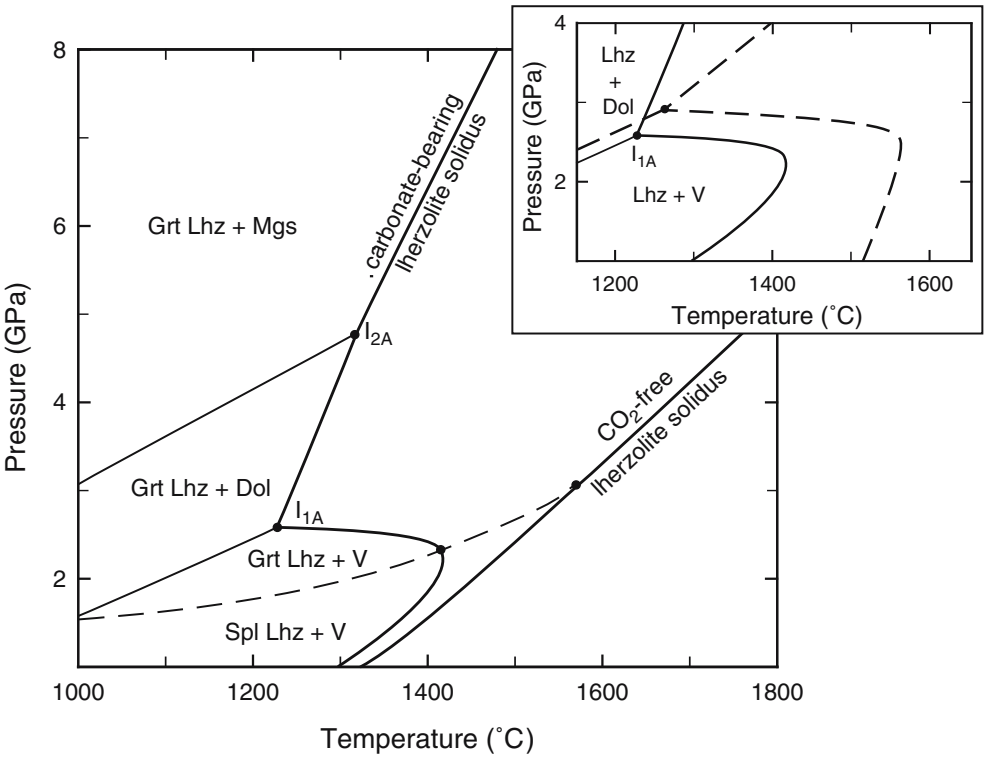

Fig. 1 Near-solidus phase relationships for lherzolite in the $CaO–MgO–Al_2O_3–SiO_2 \pm CO_2$ system after summary of Gudfinnsson and Presnall (2005). *Dashed curve* is the boundary between spinel lherzolite and garnet lherzolite. *Light solid curve* terminating at I_{1A} is the carbonation reaction stabilizing dolomite (Dol + Opx = Cpx + Ol + V). *Light solid curve* terminating at I_{2A} is the exchange reaction Mgs + Cpx = Dol + Opx that stabilizes magnesite at higher pressure in lherzolitic assemblages. Abbreviations: *Lhz* lherzolite, *Grt* garnet, *Spl* spinel, *Mgs* magnesite, *Dol* dolomite, *V* CO_2-rich vapor. *Inset* compares phase relationships in $CaO–MgO–Al_2O_3–SiO_2–CO_2$ (*solid lines*, after Gudfinnsson and Presnall 2005) with those in $CaO–MgO–SiO_2–CO_2$ (*dashed lines*, after White and Wyllie 1992)

Experimental techniques

The starting material was a 1:1:2 (molar) mixture of $CaCO_3$ (99.95% purity), MgO (99.95% purity), and SiO_2 (99.5% purity), all from Alfa Chemicals. In terms of weight percentages of the oxides, the mixture has SiO_2 46.12, MgO 15.47, CaO 21.52, and CO_2 16.89. At pressures lower than the carbonation reaction Dol + 2 Cst = Di + 2 CO_2, this mixture corresponds to diopside + 16.89 wt.% CO_2. At pressures higher than the carbonation reaction, the stable subsolidus assemblage would be diopside + dolomite + coesite (Fig. 2).

All reagents were dried prior to use: $CaCO_3$ at 300°C, MgO and SiO_2 at 1,000°C, and were stored in a desiccator over KOH before weighing. After weighing, the reagents were mixed by grinding in an agate mortar in ethyl alcohol for 30 min. The mixture was dried under a heat lamp, and stored in a desiccator prior to use.

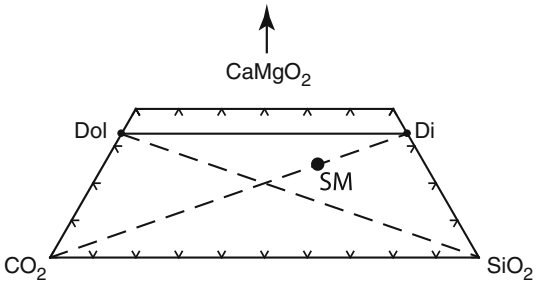

Fig. 2 Chemography of starting material (*circle*) in the ternary $CaMgO_2–SiO_2–CO_2$ (molar units)

Samples were encapsulated in triple-crimped, welded Pt capsules of 1.5 mm OD for the experiments. After approximately 3–5 mg of sample was loaded, the capsule was dried at 120°C for ~16 h, then the top of the capsule was welded shut. The sealed capsule was compressed gently into a compact cylinder in a steel die. The experiments were run in sample assemblies consisting of a semi-sintered MgO + 5% Cr_2O_3 octahedron of 18 mm edge length containing a stepped graphite furnace surrounded by a ZrO_2 sleeve. Inside the furnace, a MgO sleeve separated the capsule from the furnace, and MgO spacers above and below the capsule centered it in the assembly. A $W_{95}Re_5–W_{74}Re_{26}$ thermocouple, housed in an alumina (99.98% purity) sleeve, was inserted axially through the top MgO spacer. The same assembly was used in previous studies in this laboratory (e.g., Walter et al. 1995; Luth 1995, 2001; Knoche et al. 1999; Buob et al. 2005).

All experiments were run in the USSA-2000 split-sphere multiple-anvil apparatus in the C.M. Scarfe Laboratory for Experimental Petrology at the University of Alberta. The pressure calibration was based on experimental brackets at 1,000°C of the quartz–coesite transition in SiO_2 at 2.95 GPa (Bohlen 1984), the garnet–perovskite transition in $CaGeO_3$ at 6.1 GPa (Susaki et al. 1985), and the coesite–stishovite transition in SiO_2 at 9.1 GPa (Yagi and Akimoto 1976), as detailed in Walter et al. (1995). Based on the reproducibility of the calibration experiments, the uncertainty in pressure is estimated to be ~0.5 GPa.

Experiments were brought to run pressure, then heated at ~70°C/min to run temperature, and maintained

at ±5°C. No correction for pressure was applied to the *emf* of the thermocouple. Temperature gradients within the sample capsule are estimated to be <50°C, based on two-pyroxene geothermometry (Domanik and Luth 1999).

The experiments were quenched by turning off the power to the furnace, resulting in a temperature drop to <300°C in 2–5 s. The experiment was then decompressed over 3–6 h, depending on the pressure of the experiment. After removal from the sample assembly, the capsule was mounted in an epoxy plug using Petropoxy 154. Capsules from high-temperature, low-pressure experiments anticipated to contain a CO_2 vapor were punctured with a micro drill prior to mounting to avoid rupture of the capsule during curing of the epoxy at 120°C. After mounting, all capsules were ground on SiC sandpaper using water as a lubricant to expose a longitudinal cross-section. Initial grinding was on 240 grit paper; once the capsule wall was breached, 400 grit paper was used and the sample was vacuum-impregnated repeatedly with epoxy during the grinding to the final surface. Then the sample was ground on a 600 grit Buehler diamond disc with water, followed by lapping on a PSA-backed paper polishing pad with 0.3 μm aluminum oxide and water. The final step was on a PSA-backed fiber cloth using a paste of 0.05 μm aluminum oxide and water. Because there were no alkalis in the system to form water-soluble carbonates, it was deemed unnecessary to use water-free lubricants or solvents. After cleaning, each sample was carbon coated for examination and analysis with a JEOL 8900R electron microprobe. The textural relationships between the coexisting phases were examined using backscattered electron (BSE) imaging, and quantitative analysis was done on samples with >5 μm grain size. The quantitative analyses were done at 15 kV accelerating voltage. The sample current, as measured on a Faraday cup, was 15 nA for silicates and 5 nA for carbonates. Counting times were 20 s on peaks and 10 s on background. The data were reduced with the ZAF correction scheme provided by JEOL. Carbon (as carbonate) was calculated by stoichiometry. Quenched liquids were analyzed with 5–7 nA beam current and a 5–10 μm beam diameter, depending on the size of the melt pocket. CO_2 contents of the quenched liquids were calculated as the difference between 100% and the analysis total.

Results

The results of the experiments are summarized in Table 1, and illustrated in pressure–temperature projection in Fig. 3. The symbols in Fig. 3 omit CO_2-rich vapor, because no quench vapor deposits were found in the run products. The low-pressure subsolidus field is inferred to have vapor present, however, because of the absence of other CO_2-bearing phases (liquid or carbonate). This inference is supported by the markedly higher amount of void space in experimental charges from the low-pressure subsolidus field compared to that in charges from the Cpx + Dol + Cst field (Table 1). In the low-pressure subsolidus experiments, this void space is mostly between the capsule wall and the crystalline material, with lesser amounts interstitial in the charge. The void space is inferred to result primarily from CO_2 vapor present in the quenched experiment; only a small amount is attributable to decompression cracks based on the results from the higher-pressure subsolidus experiments in which carbonate is present (Table 1).

In most experiments containing multiple phases, the solid phases were distributed homogeneously throughout the capsule. Where present, quenched liquid occurred typically both interstitial between grains, and as segregated layers or pools at the top of the capsule. In some experiments, the carbonate phase or phases were present partially or exclusively as a selvage at the bottom of the capsule (Table 1). This texture resembles those seen in high-pressure, fluid-present experiments in the $MgO–SiO_2–H_2O$ system (Stalder and Ulmer 2001; Schmidt and Ulmer 2004). It is unclear whether this segregation is a thermal or gravitational effect, although the latter is unlikely unless the compressibility of dolomitic carbonate is greater than that of clinopyroxene. Although the compositional trends of the phases are suggestive of equilibrium, the possibility that carbonate present exclusively in a segregation at the bottom of the capsule may not be in equilibrium with liquid elsewhere in the capsule cannot be excluded.

For comparison with the present results, the previously determined reaction boundaries for Di + CO_2 = Liq at low pressure (Eggler and Rosenhauer 1978), for Di = Liq (Williams and Kennedy 1969; Boettcher et al. 1982), and for the subsolidus reactions Dol + Cst = Di + CO_2 (Luth 1995) and Arg + Mgs = Dol (Luth 2001) are shown in Fig. 3. The 1,300 K result on the latter reaction of Shirasaka et al. (2002) agrees with the curve shown within the combined uncertainties of the two studies.

The average compositions of the coexisting phases in selected experiments are presented in Table. 2, 3, and 4. The modal abundances of coexisting phases were calculated by mass balance (Table 5), using the average compositions of the phases (Table. 2, 3, 4), and the MIXING program of IGPET (Carr 2002).

The compositions of the clinopyroxenes are more magnesian than diopside (Fig. 4), even in the subsolidus regions. At pressures above the carbonation reaction, this offset to more magnesian compositions can be attributed to partitioning of Ca preferentially into the carbonate (Fig. 5). However, the offset in composition at pressures below the carbonation reaction must have a different explanation. The appearance of coesite in subsolidus experiments at $P > 3$ GPa requires that diopside dissolves incongruently into the CO_2-rich vapor. The shift in the composition of the clinopyroxene is consistent with Ca dissolving into the vapor preferentially relative to Mg, such that the relative solubility in the vapor is Ca > Mg > > Si. No precipitates from the

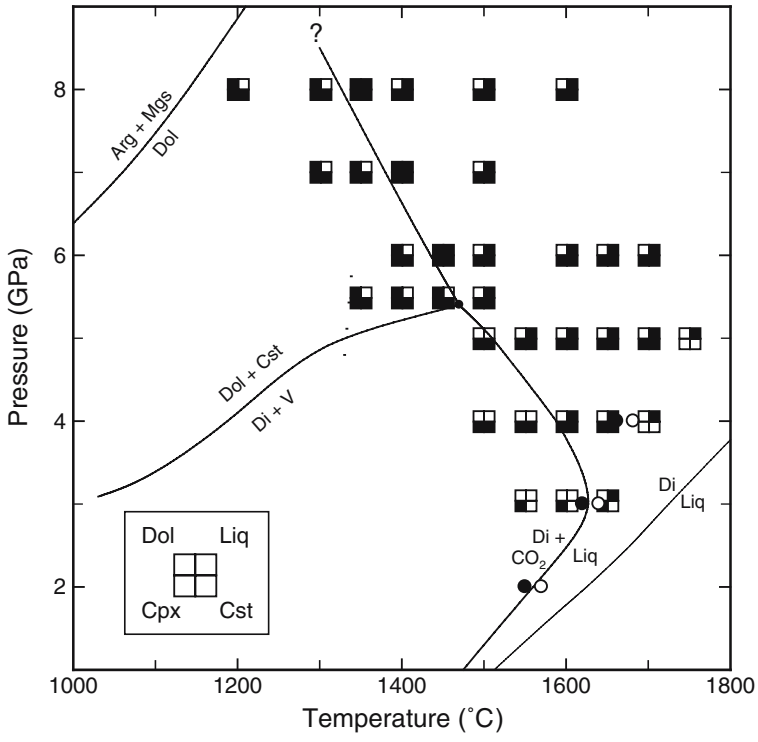

Fig. 3 Experimental results. *Filled quadrant of square* denotes presence of phase. For comparison, the volatile-free Di = Liq curve is from Williams and Kennedy (1969) and Boettcher et al. (1982), the low-pressure results for Di + CO_2 = Liq (*small circles*) are from Eggler and Rosenhauer (1978), the Dol + Cst = Di + CO_2 reaction boundary is from Luth (1995), and that of the Arg + Mgs = Dol reaction from Luth (2001)

quenched vapor were identified in BSE imaging, consistent with relatively low solubilities in the CO_2-rich fluid.

Some insight into the relative proportions of Ca and Mg in the vapor may be obtained from mass balance calculations for three experiments containing the assemblage clinopyroxene + coesite + vapor. In these calculations, $\mathbf{X}^{v}_{\mathrm{MgO}}$ and $\mathbf{X}^{v}_{\mathrm{CaO}}$ are treated as unknowns along with the mass fractions of the three phases. These calculations produce loci of possible vapor compositions for the experiments. The bands in Fig. 6 are calculated for $X^{v}_{CO_2} \geq 0.70$ using the range in analyzed composition of the clinopyroxenes from each experiment. A robust conclusion from these calculations is that the vapor is enriched significantly in Ca over Mg. A more tentative one, given the overlap in the bands, is that the Ca/Mg in the vapor decreases with both increasing temperature and increasing pressure (Fig. 6).

The appearance of coesite in supersolidus experiments at low pressures may result from incongruent

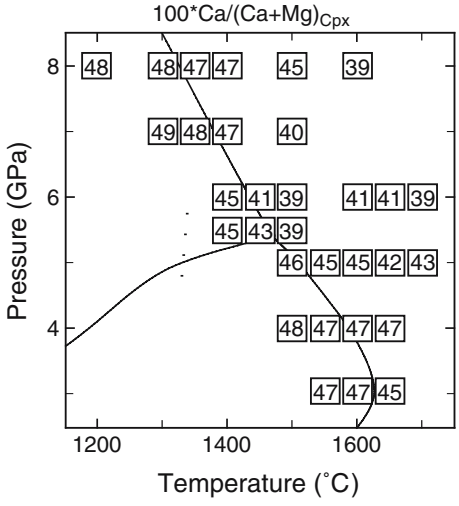

Fig. 4 Values of 100×Ca/(Ca + Mg) (molar) for clinopyroxenes as a function of pressure and temperature. For reference, the solidus curve and the Dol + Cst = Di + CO_2 reaction boundary from Fig. 3 are shown

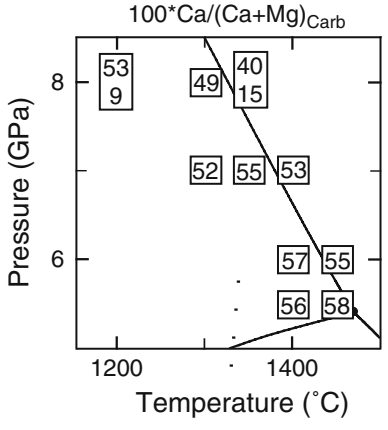

Fig. 5 Values of 100×Ca/(Ca + Mg) (molar) for crystalline carbonates in experimental products as a function of pressure and temperature. For reference, the solidus curve and the Dol + Cst = Di + CO_2 reaction boundary from Fig. 3 are shown. Note that at 8 GPa, two coexisting carbonates were found at 1,200 and 1,400°C

Table 1 Experimental runs: conditions and results

Run #	*P* (GPa)	*T* (°C)	Duration (h)	Results	Void space
1672	3	1,550	6	Cpx	35
1671	3	1,600	6	Cpx	26
1686	3	1,650	8	Cpx + qLiq (segregated at top of capsule)	27
1640	4	1,500	8	Cpx + s/a Cst	25
1659	4	1,550	8	Cpx + s/a Cst	40
1632	4	1,600	4	Cpx + s/a Cst + qLiq (segregated at top of capsule)	41
1688	4	1,600	8	Cpx + Cst + s/a qLiq (interstitial and segregated at top of capsule)	34
1633	4	1,650	4	Cpx + s/a Cst + qLiq (segregated at top of capsule)	42
1689	4	1,650	8	Cpx + qLiq (segregated at top of capsule)	11
1687	4	1,700	4	qLiq	22
1641	5	1,500	8	Cpx + Cst	19
1660	5	1,550	8	Cpx + Cst + qLiq (interstitial and segregated at top of capsule)	17
1635	5	1,600	4	Cpx + Cst + qLiq (interstitial and segregated along side of capsule)	27
1613	5	1,650	2	Cpx + Cst + qLiq (interstitial and segregated at top of capsule)	4
1619	5	1,700	2	Cpx + Cst + qLiq (segregated at top of capsule)	2
1614	5	1,750	1	qLiq	30
1690	5.5	1,350	8	Cpx + Cst + Dol. Very fine-grained	4
1673	5.5	1,400	8	Cpx + Cst + Dol + s/a qLiq	< 1
1691	5.5	1,400	8	Cpx + Cst + Dol	< 1
1705	5.5	1,400	24	Cpx + Cst + Dol	1
1706	5.5	1,450	8	Cpx + Cst + Dol	11
1675	5.5	1,500	8	Cpx + Cst + qLiq (mostly interstitial, small segregation at top of capsule)	< 1
1642	6	1,400	24	Cpx + Dol + Cst. Selvage of Dol at bottom of capsule	< 1
1644	6	1,450	24	Dol-rich selvage at bottom (+ Cst + Cpx), Cst + Cpx + interstitial qLiq in most of capsule. Thin qLiq segregation at top.	3
1637	6	1,500	8	Cpx + Cst + qLiq (interstitial and segregated at sides)	< 1
1615	6	1,600	4	Cpx + Cst + qLiq (interstitial and segregated at top and sides)	2
1616	6	1,650	2	Cpx + Cst + qLiq (interstitial and segregated at top)	< 1
1617	6	1,700	2	Cpx + Cst + qLiq (interstitial and segregated at top)	7
1692	7	1,300	24	Cpx + Dol + Cst. Selvage of Dol at bottom of capsule	2
1643	7	1,350	24	Cpx + Dol + Cst. Very fine-grained	< 1
1618	7	1,400	8	Cpx + Dol + Cst + s/a qLiq (interstitial and as small segregation at top of capsule). Dol as selvage at bottom	< 1
1693	7	1,500	6	Cpx + Cst + qLiq (interstitial and as segregations at top and sides)	2
1611	8	1,200	8	Cpx + Cst + Dol + Mgs. Very fine-grained	< 1
1610	8	1,300	8	Cpx + Cst + Dol. Dol throughout and as selvage at bottom	1
1661	8	1,350	24	Cpx + Cst + Dol + Mgs + qLiq (interstitial and as segregation at top). Dol and Mgs in selvage at bottom	< 1
1598	8	1,400	8	Cpx + Cst + qLiq (interstitial).	1
1597	8	1,500	6	Cpx + Cst + qLiq (interstitial)	2
1595	8	1,600	4	Cpx + Cst + qLiq (interstitial)	< 1

Void space calculated from gray-scale backscattered electron images of capsule cross-section
s/a Small amount, *Cpx* clinopyroxene, *Cst* coesite, *Dol* dolomite, *Mgs* magnesite, *qLiq* quench liquid

Table 2 Microprobe analyses of clinopyroxene

Expt#	1672	1671	1686	1640	1659	1688	1689	1641
P (GPa)	3	3	3	4	4	4	4	5
T (°C)	1,550	1,600	1,650	1,500	1,550	1,600	1,650	1,500
t (h)	6	6	8	8	8	8	8	8
N	9	21	5	18	19	15	9	19
Wt. %								
SiO_2	55.04 (0.26)	55.06 (0.34)	55.32 (0.14)	55.70 (0.34)	54.94 (0.41)	55.12 (0.31)	55.03 (0.41)	56.14 (0.53)
CaO	24.66 (0.86)	24.74 (0.52)	23.93 (0.10)	25.18 (0.21)	24.57 (0.36)	24.58 (0.31)	24.11 (0.17)	24.31 (0.43)
MgO	19.85 (0.62)	19.82 (0.49)	20.68 (0.09)	19.62 (0.25)	19.90 (0.29)	19.98 (0.17)	19.41 (0.20)	20.19 (0.38)
Total	99.55 (0.42)	99.62 (0.48)	99.94 (0.14)	100.50 (0.42)	99.41 (0.43)	99.68 (0.23)	98.93 (0.52)	100.64 (0.49)
Cations/6 oxygens								
Si	1.9883	1.9879	1.9862	1.9938	1.9874	1.9879	1.9976	2.0000
Ca	0.9546	0.9571	0.9206	0.9656	0.9524	0.9499	0.9254	0.9279
Mg	1.0688	1.0671	1.1070	1.0468	1.0728	1.0743	1.0437	1.0720
Total	4.0117	4.0121	4.0138	4.0062	4.0126	4.0121	3.9668	4.0000

Expt#	1660	1635	1613	1673	1705	1706	1675	1642
P (GPa)	5	5	5	5.5	5.5	5.5	5.5	6
T (°C)	1,550	1,600	1,650	1,400	1,400	1,450	1,500	1,400
t (h)	8	4	2	8	24	8	8	24
N	15	14	11	13	19	24	14	14
Wt.%								
SiO_2	55.05 (0.55)	55.18 (0.42)	55.12 (0.15)	55.21 (0.26)	55.91 (0.35)	56.22 (0.47)	55.38 (0.29)	55.96 (0.62)
CaO	23.32 (0.46)	23.45 (0.39)	22.43 (0.54)	22.36 (0.40)	23.14 (0.31)	22.46 (0.78)	20.91 (0.63)	23.77 (0.27)
MgO	20.71 (0.32)	20.96 (0.26)	21.84 (0.44)	21.52 (0.37)	20.48 (0.26)	21.05 (0.57)	23.20 (0.50)	20.66 (0.23)
Total	99.09 (0.35)	99.59 (0.38)	99.39 (0.20)	99.09 (0.30)	99.53 (0.40)	99.73 (0.37)	99.49 (0.30)	100.39 (0.65)
Cations/6 oxygens								
Si	1.9903	1.9857	1.9823	1.9901	2.0071	2.0093	1.9808	1.9964
Ca	0.9034	0.9041	0.8645	0.8637	0.8901	0.8600	0.8014	0.9084
Mg	1.1161	1.1245	1.1709	1.1561	1.0957	1.1213	1.2370	1.0988
Total	4.0097	4.0143	4.0177	4.0099	3.9929	3.9907	4.0192	4.0036

Expt#	1644	1637	1615	1616	1617	1692	1643	1618
P (GPa)	6	6	6	6	6	7	7	7
T (°C)	1,450	1,500	1,600	1,650	1,700	1,300	1,350	1,400
t (h)	24	8	4	2	2	24	24	8
N	20	11	20	23	9	10	12	26
Wt.%								
SiO_2	55.27 (0.20)	55.94 (0.35)	56.33 (0.19)	56.52 (0.18)	53.80 (0.62)	55.18 (0.36)	55.58 (0.57)	56.06 (0.35)
CaO	21.84 (0.41)	20.96 (0.58)	21.52 (0.37)	21.04 (0.32)	20.49 (0.39)	24.81 (0.14)	24.80 (0.28)	24.05 (0.27)
MgO	22.31 (0.35)	23.25 (0.40)	21.85 (0.30)	22.19 (0.33)	22.83 (0.28)	19.38 (0.22)	19.70 (0.17)	19.82 (0.30)
Total	99.42 (0.27)	100.15 (0.43)	99.70 (0.29)	99.75 (0.23)	97.12 (0.42)	99.37 (0.29)	100.08 (0.45)	99.93 (0.43)
Cations/6 oxygens								
Si	1.9833	1.9861	2.0082	2.0107	1.9733	1.9964	1.9957	2.0090
Ca	0.8398	0.7973	0.8220	0.8020	0.8050	0.9618	0.9542	0.9233
Mg	1.1935	1.2304	1.1615	1.1765	1.2484	1.0453	1.0544	1.0588
Total	4.0167	4.0139	3.9918	3.9893	4.0267	4.0036	4.0043	3.9910

Expt#	1693	1611	1610	1661	1598	1597	1595
P (GPa)	7	8	8	8	8	8	8
T (°C)	1,500	1,200	1,300	1,350	1,400	1,500	1,600
t (h)	6	8	8	24	8	6	4
N	18	8	13	18	3	13	20
Wt.%							
SiO_2	55.69 (0.51)	54.42 (1.54)	54.80 (0.53)	54.91 (0.19)	54.04 (0.44)	54.63 (0.51)	54.92 (0.37)
CaO	21.10 (1.65)	24.66 (0.84)	25.35 (0.15)	24.41 (0.18)	24.74 (0.25)	23.63 (0.78)	21.01 (1.03)
MgO	22.51 (1.27)	19.15 (0.52)	19.55 (0.21)	19.78 (0.10)	20.24 (0.36)	21.08 (0.60)	23.18 (0.83)
Total	99.30 (0.32)	98.22 (0.57)	99.71 (0.40)	99.11 (0.28)	99.02 (0.48)	99.34 (0.49)	99.11 (0.31)

Table 2 (Contd.)

Expt#	1693	1611	1610	1661	1598	1597	1595
Cations/6 oxygens							
Si	1.9945	1.9934	1.9817	1.9911	1.9680	1.9745	1.9744
Ca	0.8096	0.9677	0.9824	0.9485	0.9653	0.9149	0.8092
Mg	1.2015	1.0455	1.0541	1.0694	1.0986	1.1360	1.2420
Total	4.0055	4.0066	4.0183	4.0089	4.0320	4.0255	4.0256

N number of analyses. Numbers in parentheses are 1 s.d. of the mean

Table 3 Microprobe analyses of carbonates

Expt#	1673	1691	1705	1706	1642	1644	1692	1643
P (GPa)	5.5	5.5	5.5	5.5	6	6	7	7
T (°C)	1,400	1,400	1,400	1,450	1,400	1,450	1,300	1,350
t (h)	8	8	24	8	24	24	24	24
N	21	11	22	15	13	15	21	13
Wt.%								
MgO	19.68 (0.78)	18.59 (0.25)	19.80 (0.53)	18.40 (1.40)	19.47 (1.02)	20.01 (0.54)	21.35 (0.79)	20.23 (0.55)
CaO	34.94 (1.00)	36.73 (0.50)	34.67 (1.02)	35.86 (2.40)	35.71 (1.24)	34.59 (0.81)	32.00 (0.81)	34.19 (1.09)
CO_2	45.38 (0.96)	44.68 (0.56)	45.54 (0.85)	45.74 (1.25)	44.81 (0.84)	45.39 (0.52)	46.65 (0.66)	45.58 (0.95)
Total	100.00	100.00	100.00	100.00	100.00	100.00	100.00	100.00

Expt#	1618	1611	1611	1610	1661	1661
P (GPa)	7	8	8	8	8	8
T (°C)	1,400	1,200	1,200	1,300	1,350	1,350
t (h)	8	8	8	8	24	24
N	14	3	11	8	18	13
Wt.%		(Low Ca)	(High Ca)		(Low Ca)	(High Ca)
MgO	21.15 (0.53)	43.00 (1.25)	21.10 (2.01)	23.15 (1.01)	39.77 (0.68)	27.25 (0.55)
CaO	33.64 (0.83)	5.65 (1.52)	32.94 (2.73)	31.09 (1.40)	9.39 (0.69)	24.82 (0.64)
CO_2	45.21 (0.88)	51.34 (0.28)	45.96 (1.79)	45.76 (1.12)	50.84 (0.34)	47.93 (0.50)
Total	100.00	100.00	100.00	100.00	100.00	100.00

N number of analyses averaged. Numbers in parentheses are 1 s.d. of the mean

dissolution into the CO_2 vapor, as outlined above for subsolidus conditions. An alternative (or supplemental) explanation is that the clinopyroxene dissolves incongruently into the liquid, consistent with reaction of the CO_2 to form calcium and magnesium carbonate complexes. The changing composition of the liquid with pressure has textural effects as well: at 3 GPa, the melt quenches to glass (Fig. 7a), but at higher pressures, the liquid quenches into dendritic crystals (Fig. 7b, c, d) that progressively coarsen with increasing pressure. By 6 GPa, the quenched liquid is comprised of blades of carbonate-rich material with interstitial thin stringers of pyroxene (Fig. 7e, f). Broad-beam microprobe analyses confirm a gradual change in the composition of the liquid at pressures above 3 GPa. The silica content of the liquid near the solidus drops from 49 wt.% at 3 GPa to 27 wt.% at 4 GPa to 2 wt.% at 5.5 GPa (Fig. 8). Based on the calculated CO_2 content as well as the silica content, the liquid changes from a silicate melt with ~10 wt.% dissolved CO_2 at 3 GPa through a transitional stage with 26–40 wt.% CO_2, to a *bona fide* carbonatitic melt with very low SiO_2 content and CO_2 near 44 wt.% at 5.5 GPa, where the subsolidus carbonation reaction intersects the solidus (Fig. 9). This change is accompanied by an increase in the Ca# ($100\times Ca/(Ca+Mg)_{molar}$) of the near-solidus melt from 60 at 3 GPa to 74 at 4 GPa, then a decrease to 65 by 5.5 GPa (Fig. 10). With further increase in pressure, the Ca# gradually increases to 68 at 8 GPa. The evolution in the composition of the near-solidus melts with pressure may be illustrated by projecting them onto the CaO–MgO–SiO_2 face of the CaO–MgO–SiO_2–CO_2 tetrahedron (Fig. 11). This projection also graphically illustrates the reduction of silica content of the liquid with increasing pressure.

At several pressures, the evolution of the composition of the melt with increasing temperature can be documented (Fig. 12). The 4 and 5 GPa trends converge at the highest temperature points in Fig. 12, because those experiments contained only quenched liquid (Fig. 3). The SiO_2 content of the initial melts systematically decreases with increasing pressure as outlined above. Interestingly, the two melt compositions at 8 GPa differ only in Ca/Mg; both contain little

Table 4 Microprobe analyses of quench liquids

Expt#	1686	1632	1688	1633	1689	1687	1660	1635
P (GPa)	3	4	4	4	4	4	5	5
T (°C)	1,650	1,600	1,600	1,650	1,650	1,700	1,550	1,600
t (h)	8	4	8	4	8	4	8	4
N	17	10	5	13	15	15	12	6
Wt.%								
MgO	13.27 (0.29)	14.65 (0.54)	9.31 (1.53)	13.47 (0.94)	10.03 (1.52)	16.81 (0.11)	11.42 (0.59)	15.71 (0.77)
CaO	28.03 (0.20)	26.03 (1.06)	37.66 (2.35)	26.27 (1.70)	31.98 (2.00)	23.71 (0.14)	40.47 (0.98)	34.79 (0.56)
SiO_2	49.30 (0.34)	50.17 (2.02)	27.16 (4.70)	49.95 (2.64)	41.74 (1.79)	50.03 (0.28)	8.01 (2.97)	17.73 (1.10)
Total	90.60 (0.55)	90.85 (1.43)	74.13 (3.86)	89.69 (1.94)	83.75 (1.31)	90.55 (0.32)	59.91 (2.53)	68.23 (1.48)
CO_2^a	9.40 (0.55)	9.15 (1.43)	25.87 (3.86)	10.31 (1.94)	16.25 (1.31)	9.45 (0.32)	40.09 (2.53)	31.77 (1.48)

Expt#	1613	1614	1675	1644	1637	1615	1616	1617
P (GPa)	5	5	5.5	6	6	6	6	6
T (°C)	1,650	1,750	1,500	1,450	1,500	1,600	1,650	1,700
t (h)	2	1	8	24	8	4	2	2
N	7	12	12	12	16	10	13	12
Wt.%								
MgO	17.79 (0.4)	15.76 (0.28)	15.26 (0.65)	15.55 (0.53)	16.77 (0.36)	18.62 (0.44)	18.46 (0.63)	18.25 (0.45)
CaO	27.33 (0.36)	23.07 (0.32)	38.78 (0.83)	37.87 (1.13)	36.03 (0.52)	32.24 (0.30)	31.59 (0.55)	25.86 (0.41)
SiO_2	34.30 (0.40)	48.28 (0.25)	2.35 (0.74)	2.34 (0.83)	3.77 (0.76)	17.08 (0.97)	19.16 (1.97)	38.17 (1.12)
Total	79.42 (0.84)	87.12 (0.60)	56.39 (0.72)	55.77 (0.79)	56.57 (0.65)	67.94 (1.15)	69.21 (1.38)	82.28 (0.47)
CO_2^a	20.58 (0.84)	12.89 (0.60)	43.61 (0.72)	44.23 (0.79)	43.43 (0.65)	32.06 (1.15)	30.79 (1.38)	17.72 (0.47)

Expt#	1618	1693	1661	1595
P (GPa)	7	7	8	8
T (°C)	1,400	1,500	1,350	1,600
t (h)	8	6	24	4
N	4	13	6	10
Wt.%				
MgO	14.61 (1.09)	17.12 (0.22)	13.75 (1.39)	18.8 (2.73)
CaO	40.20 (1.70)	34.27 (0.39)	40.37 (1.44)	36.03 (4.19)
SiO_2	0.57 (0.32)	5.17 (0.98)	0.51 (0.25)	0.77 (0.88)
Total	55.38 (0.43)	56.56 (0.82)	54.64 (1.06)	55.59 (2.08)
CO_2^a	44.62 (0.43)	43.44 (0.82)	45.36 (1.06)	44.41 (2.08)

N number of analyses averaged. Numbers in parentheses are 1 s.d. of the mean
[a]CO_2 was calculated as the difference between the analysis total and 100%

SiO_2 (1%, Fig. 8), despite the fact that the higher temperature experiment being ~275°C above the solidus. Over a similar temperature range, the liquids at 6 GPa change composition much more dramatically, especially with respect to the silica concentrations (2–38 wt.%). Even more extensive changes from carbonatite to silicate melts are seen over smaller temperature ranges at 4 and 5 GPa, although the near-solidus melt at these lower pressures contains more silica than those at higher pressures.

The divergence of the compositions of the clinopyroxenes, carbonates, and especially the liquids from a molar Ca:Mg of unity means that the system cannot be considered as a three-component system ($CaMgO_2$–SiO_2–CO_2) for chemographic purposes, but must be considered in the full quaternary (CaO–MgO–SiO_2–CO_2). This conclusion in turn means that the solidus assemblage of clinopyroxene + carbonate + coesite + liquid is divariant, rather than univariant, and the phase relationships determined in this study are valid strictly for only this bulk composition.

Discussion

Comparison with previous studies

Eggler and Rosenhauer (1978) experimentally determined the phase relationships in the $CaMgSi_2O_6$–H_2O–CO_2 system from 2 to 4 GPa, including the $CaMgSi_2O_6$–CO_2 sideline (Fig. 3). They found the Di + CO_2 = Liq reaction at 1,565° at 2 GPa. At 3 GPa, an experiment at 1,620° contained crystalline diopside and crystals interpreted to have quenched from a melt, whereas an experiment at 1,640°C contained glass and quench crystals. At 4 GPa, a 1,660° experiment contained crystalline diopside and quench crystals, whereas an experiment 20°C higher contained only quench crystals. In both cases, the authors interpreted the lower-temperature experiment to be subsolidus. They attributed the presence of quench crystals in subsolidus experiments to result from temperature gradients across the sample, incongruent melting of diopside, and/or the

Table 5 Calculated modal proportions of phases present

Expt#	*P* (GPa)	*T* (°C)	*T* (h)	Cpx (Weight %)	Carb	Cst	qLiq	Vapor
1686	3	1,650	8	58	0	0	28	14
1688	4	1,600	8	73	0	3	10	14
1689	4	1,650	8	74	0	3	11	15
1660	5	1,550	8	66	0	8	15	11
1635	5	1,600	4	55	0	11	25	9
1613	5	1,650	2	20	0	14	62	4
1673	5.5	1,400	8	38	37	25	0	0
1705	5.5	1,400	24	38	37	25	0	0
1706	5.5	1,450	8	39	37	24	0	0
1675	5.5	1,500	8	47	0	20	30	4
1642	6	1,400	24	37	37	26	0	0
1644	6	1,450	24	38	28	25	10	0
1637	6	1,500	8	38	0	24	39	0
1615	6	1,600	4	24	0	24	52	0
1616	6	1,650	2	23	0	23	54	0
1617	6	1,700	2	3	0	14	81	3
1692	7	1,300	24	40	36	24	0	0
1643	7	1,350	24	38	37	25	0	0
1618	7	1,400	8	38	37	25	0	0
1693	7	1,500	6	39	0	22	39	0
1611	8	1,200	8	39	36	25	0	0
1610	8	1,300	8	38	37	25	0	0
1661	8	1,350	24	40	14	24	22	0
1595	8	1,600	4	36	0	26	38	0

Calculated with MIXING sub-program of IGPET (Carr 2002)

presence of H_2O. The 3 GPa results of the present study define a solidus consistent with that of Eggler and Rosenhauer (1978), but the 4 GPa results appear to be inconsistent (Fig. 3). If the 4 GPa results of Eggler and Rosenhauer are interpreted to constrain the location of a liquidus, however, their results agree with the location of the liquidus determined in the present study. This interpretation means that the quench crystals in their lower-temperature experiments at 3 and 4 GPa quenched from an equilibrium liquid. They did not report coesite in their subliquidus experiment, however, suggesting there is still a discrepancy between the results of the two studies. It is possible that coesite was overlooked in their run products, given its low modal abundance (~3 wt.%) at these conditions (Table 5). Alternatively, this discrepancy may be a result of differences in the pressure calibrations of the two experimental apparatus, given that 4 GPa is the lowest pressure at which coesite was observed in the present study.

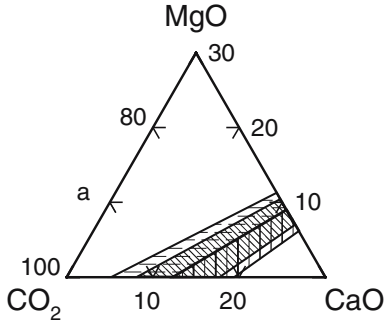

Fig. 6 Calculated range of composition of vapor in three experiments containing Cpx + Cst + V, plotted in the CO_2-rich corner of the CaO–MgO–CO_2 ternary (wt.%). Each band is calculated based on the range of composition of the clinopyroxene as determined by electron microprobe analyses. *Horizontal dashed lines* 4 GPa, 1,500°C experiment; *diagonal ruled lines* 4 GPa, 1,550°C experiment; *Vertical ruled lines* 5 GPa, 1,500°C

Eggler and Rosenhauer (1978) also studied the solubility of diopside in both H_2O and CO_2 vapor at 2–3 GPa. They found in both cases that diopside dissolved congruently, with substantially higher solubility in H_2O than in CO_2. The solubility of $CaMgSi_2O_6$ in H_2O vapor is 9.5 ± 1.5 wt.% at 2 GPa and 1,200°C, and increases to 11.2 ± 1.5 wt.% at 3 GPa and 1,180°C. In contrast, they found the solubility of $CaMgSi_2O_6$ in CO_2 vapor to be 0.2 ± 0.2 wt.% at 2 GPa and 1,300°C. The present study does not offer any quantitative constraints on the solubility of diopside in the vapor, but does show that the dissolution becomes incongruent at higher pressures as described above.

The 6 GPa results of Luth (1995) for the reaction Dol + 2 Cst = Di + 2 CO_2 are not consistent with the present study, as they should have produced melting rather than a bracket on the decarbonation reaction. I attribute this discrepancy to a combination of the use of powder XRD to monitor reaction progress in my previous study, and my inability to recognize quenched carbonate melt in grain mounts of those experiments with the ARL SEMQ microprobe used for that study. In the present study, a longitudinal slice through the entire capsule was examined with the JEOL 8900R electron microprobe, which has much better backscatter electron imaging capabilities. It is worth noting that the Ca/(Ca + Mg) of the "carbonate" at 6 GPa, 1,500°C reported in Luth (1995) is consistent with the composition of quenched carbonate-rich melt from the same conditions in the present study.

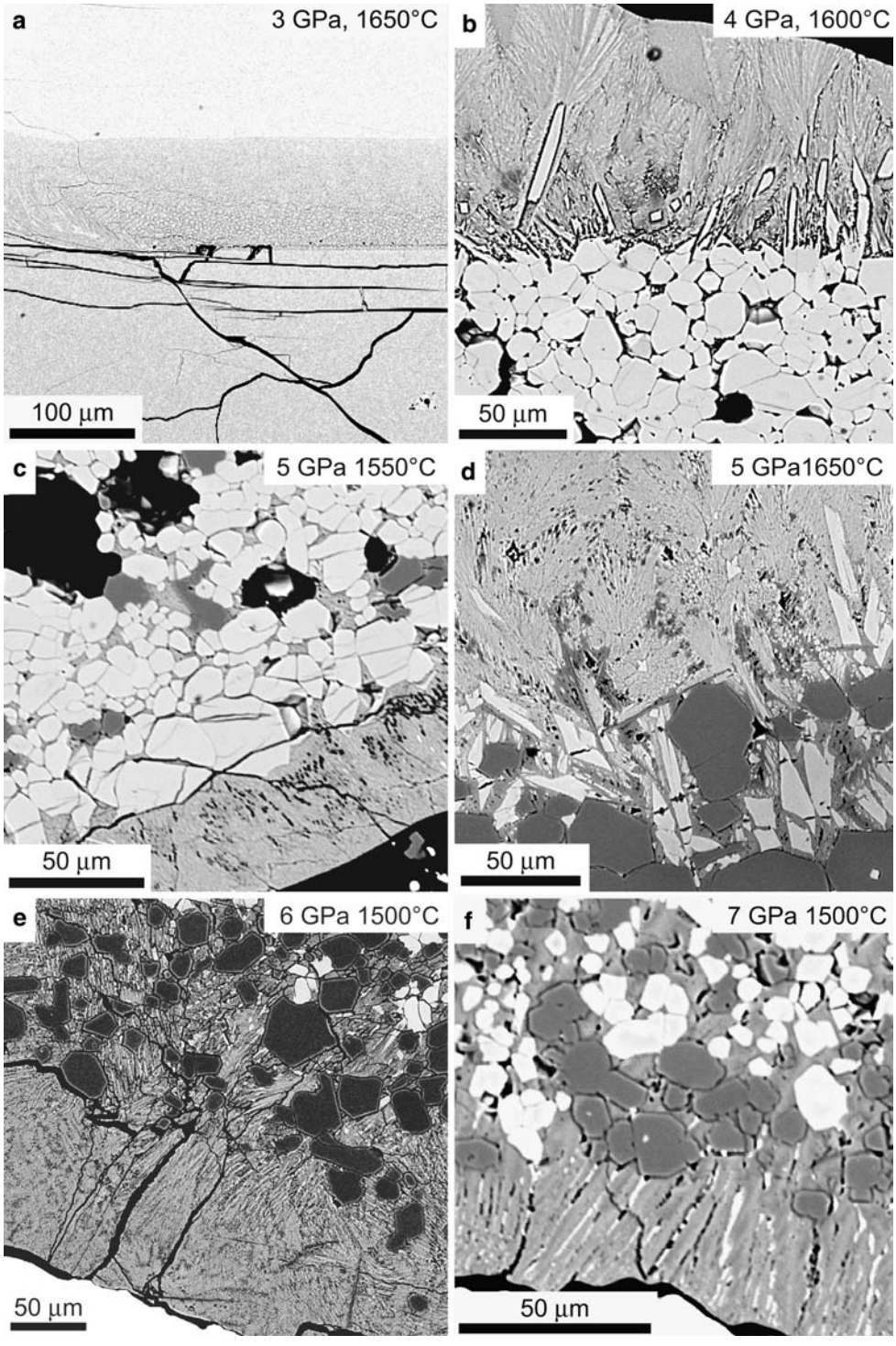

Fig. 7 Backscattered electron images of textures of experiments with quenched liquid as a function of increasing pressure. **a** 3 GPa experiment with crystalline clinopyroxene (lower third of figure), quenched liquid as homogeneous glass above. **b** 4 GPa experiment with granular crystalline clinopyroxene in lower portion of figure with quenched glass, showing dendritic quench crystals, above. **c** 5 GPa experiment showing quench liquid rim (*lower right*) adjacent to clinopyroxene (*light gray*) and coesite (*medium gray*). *Black areas* are voids. **d** Higher temperature experiment at 5 GPa showing development of quench texture in liquid. **e** 6 GPa experiment with development of two phases in quench liquid (*lighter stringers* are pyroxene). Crystalline phases are coesite (*dark gray*) and clinopyroxene (*light gray*). **f** Coarse quench crystallization in quench liquid from 7 GPa. Crystalline phases as in (**e**)

The shape of solidi: the peridotite case

The gradual decrease in the temperature of the solidus in the Di–CO_2 system contrasts markedly with the much more abrupt decrease in the solidus temperature in the lherzolite + CO_2 system (Fig. 13). It has been known since the pioneering studies in the 1970s (Eggler 1974, 1976, 1978; Wyllie and Huang 1975, 1976) that the temperature of the solidus in lherzolite–CO_2 systems decreases dramatically at ~2.5 GPa. This decrease has been attributed to a marked change in the nature of the near-solidus melt, from "basaltic"—silicate-rich melts with <10 wt.% CO_2 at pressures of 2 GPa to "carbonatitic" or "calcio-carbonatitic" melts with >40 wt.% CO_2 at the point I_{1A} in Fig. 1 where the subsolidus carbonation reaction intersects the solidus (White and Wyllie 1992). This change in the composition of the near-solidus melt reflects a rapid change in the

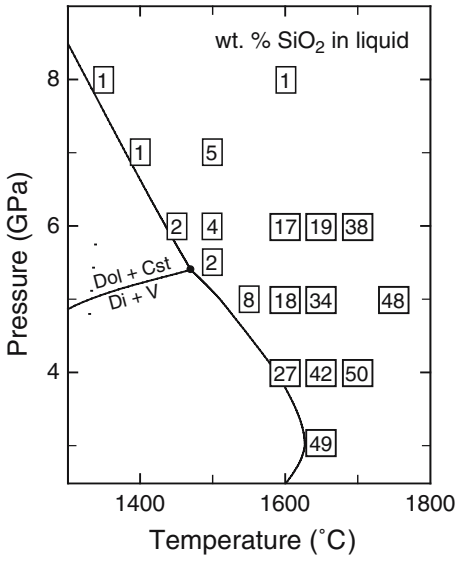

Fig. 8 Silica content of the quenched liquid (in wt.%)

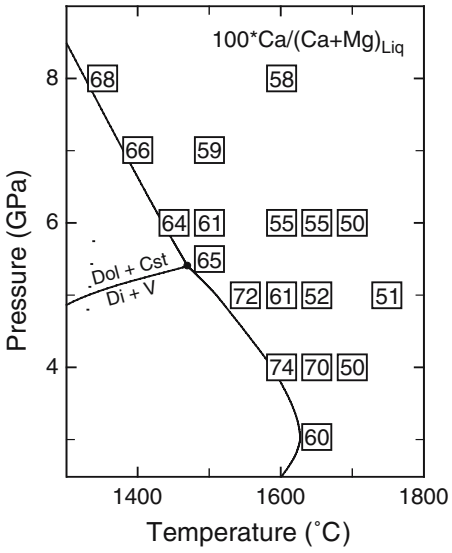

Fig. 10 Values of 100×Ca/(Ca + Mg) for quenched liquid

liquidus phase relationships over this pressure interval, such that carbonatitic melts, which are stable at lower pressures coexisting with olivine and clinopyroxene, become stable coexisting with olivine and both pyroxenes (cf. review by Moore and Wood 1998). White and Wyllie (1992) emphasized that viewing this change as merely an increase in solubility of CO_2 in the low-pressure liquid is not appropriate because of the radical change in the composition of the liquid.

Subsequent studies have confirmed the carbonate-rich nature of melts above the point I_{1A}. Moore and Wood (1998) found that a liquid in equilibrium with Ol + Opx + Cpx in the CaO–MgO–SiO_2–CO_2 system at 3 GPa contains 36 wt.% CaO, 15 wt.% MgO, 4 wt.% SiO_2. Assuming the remainder is CO_2 yields ~44 wt.% CO_2. In the CaO–MgO–Al_2O_3–SiO_2–CO_2 study of Dalton and Presnall (1998), liquid in equilibrium with Ol + Opx + Cpx + Grt + Dol at 3 GPa, 1,245°C contains 33 wt.% CaO, 17 wt.% MgO, <1 wt.% Al_2O_3, 5 wt.% SiO_2, and 44 wt.% CO_2. The liquid remains carbonate-rich and silicate-poor well above the solidus: Gudfinnsson and Presnall (2005) found similar liquids at 1,400 and 1,450°C at 3.2 GPa, and only at 1,550°C did they find a more silicic liquid, with 19 wt.% CaO, 24% MgO, 6 wt.% Al_2O_3, 35 wt.% SiO_2, and only 15 wt.% CO_2.

The melting reactions of volatile-free lherzolite and carbonated lherzolite are quite different. Although much of the work on solidus melting reactions of lherzolite has focused on spinel lherzolites, Walter (1998) determined

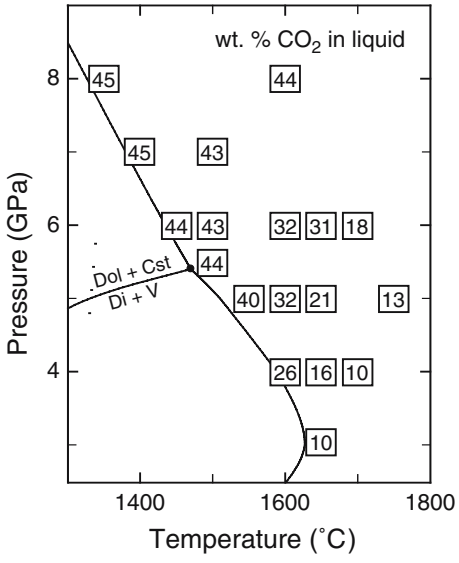

Fig. 9 Calculated CO_2 content of the liquid (in wt.%). CO_2 calculated by difference

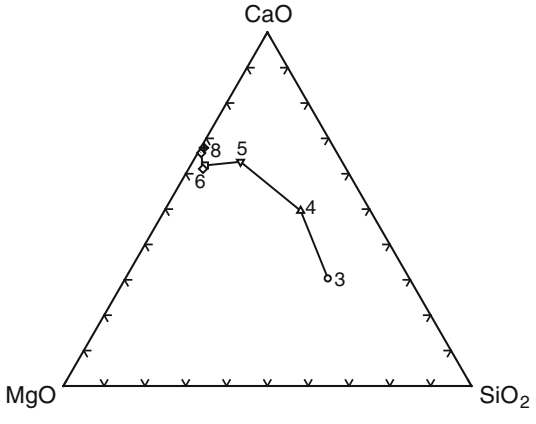

Fig. 11 Composition of near-solidus melts projected into the CaO–MgO–SiO_2 ternary (molar units). Number next to each symbol is the pressure in GPa. Unnumbered symbol between 5 and 6 is the 5.5 GPa melt; unnumbered symbol between 6 and 8 is the 7 GPa melt

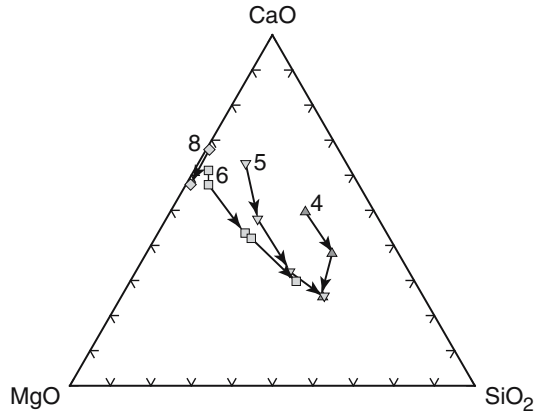

Fig. 12 Trends of liquid composition with increasing temperature projected into the CaO–MgO–SiO_2 (molar units) system. The number next to each trend is the pressure in GPa; the *arrows point* in the direction of *increasing* temperature

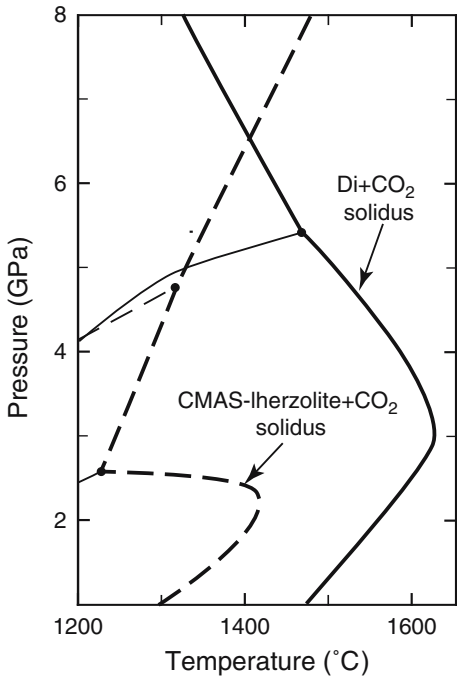

Fig. 13 Comparison of solidus for CMAS model lherzolite + CO_2 (*heavy dashed lines*, after Gudfinnsson and Presnall 2005) to solidus for Di + CO_2 (*solid lines*, this study)

the melting reactions in a natural lherzolite at 3 and 7 GPa. Wallace and Green (1988), Dalton and Wood (1993), Sweeney (1994), and Hirose (1997) all studied aspects of the melting of carbonated peridotite, but no data are available on the compositions of subsolidus minerals to constrain melting reactions. Therefore, the results of Walter (1998) must be compared to those of Dalton and Presnall (1998) in the CaO–MgO–Al_2O_3–SiO_2–CO_2 system (Table 6). In the absence of carbonate, clinopyroxene and garnet dominate the minerals reacting to produce melt, whereas carbonate and orthopyroxene dominate in the carbonated case. Once carbonate becomes stable in the subsolidus, it plays a major role in the melting reaction, and consequently in the nature of the melt produced.

The shape of solidi: Di–CO_2

The Di–CO_2 system differs from the carbonated lherzolite systems by a more gradual decrease in the temperature of the solidus in the former system, which continues above the point where the solidus intersects the subsolidus carbonation curve (Fig. 13). The near-solidus melts (Figs. 8, 9) change from relatively siliceous, with CO_2 contents near 10 wt.% at 3 GPa progressively to lower silica, higher CO_2 until by 5.5 GPa, where the carbonation reaction intersects the solidus, the melt is carbonatitic, with SiO_2 contents <5 wt.%. As pressure increases further, the near-solidus melt remains carbonatitic, with a systematic shift to more Ca-rich compositions from 5.5 to 8 GPa.

Why is there a gradual change in the temperature of the solidus in this system, rather than something more abrupt as in the model lherzolitic system? The higher pressure of the transition from silicic to carbonatitic

Table 6 Solidus melting reactions of garnet lherzolite and carbonated garnet lherzolite

P (GPa)	Reaction	Reference
Natural garnet lherzolite		
3	0.81 Cpx + 0.30 Grt + 0.08 Ol = 1 Liq + 0.19 Opx	1
7	0.50 Cpx + 0.26 Ol + 0.24 Grt = 1 Liq	1
Carbonated garnet lherzolite in CMAS–CO_2		
3	0.95 Dol + 0.43 Opx + 0.01 Grt = 1 Liq + 0.26 Cpx + 0.11 Ol	2
3.5	0.94 Dol + 0.44 Opx + 0.01 Grt = 1 Liq + 0.25 Cpx + 0.14 Ol	2
4	0.95 Dol + 0.29 Opx + 0.01 Grt = 1 Liq + 0.13 Cpx + 0.13 Ol	2
5	1.08 Cpx + 0.88 Mgs = 1 Liq + 0.77 Opx + 0.14 Ol + 0.06 Grt	2
6	1.10 Cpx + 0.86 Mgs = 1 Liq + 0.78 Opx + 0.14 Ol + 0.02 Grt	2
7	1.07 Cpx + 0.88 Mgs + 0.01 Grt = 1 Liq + 0.86 Opx + 0.10 Ol	2

1 Walter 1998; *2* Dalton and Presnall 1998. Reactions recalculated to 1 g Liq
Cpx clinopyroxene, *Dol* dolomite, *Grt* garnet, *Liq* liquid, *Mgs* magnesite, *Ol* olivine, *Opx* orthopyroxene

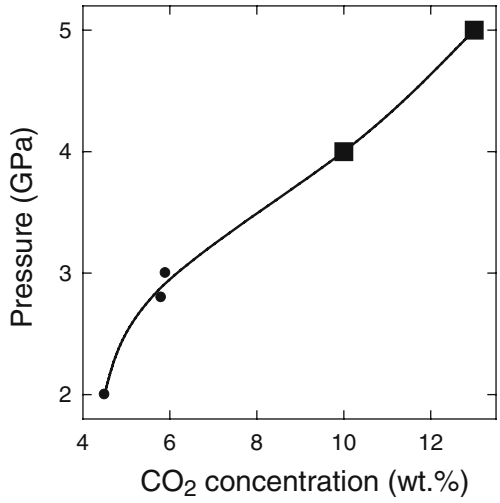

Fig. 14 Concentration of CO_2 dissolved in diopside liquid coexisting with CO_2-rich vapor. *Small circles* from summary of Rai et al. (1983), with original data sources: 2 GPa, 1,650°C from Rai et al. (1983); 2.8 GPa, 1,650°C from Mysen et al. (1976); 3 GPa, 1,700°C from Brey and Green (1976). *Large squares* this study, calculated by difference

melts may mean that the increasing solubility of CO_2 in the silicate melt with increasing pressure may play more of a role in this system than in lherzolitic systems. For example, CO_2 solubilities in basaltic melts just below the solidus 'ledge' are ~2–4 wt.% (cf. review by Holloway and Blank 1994). So in the case of melts produced from the partial melting of lherzolite, the pressure where the change from basaltic to carbonatitic melts occurs is sufficiently low that solubility of CO_2 is low below the 'ledge', and there is an abrupt change in the nature of the melt once a carbonate mineral is a stable subsolidus phase that participates in the melting reaction.

The solubility of CO_2 in liquid of diopside composition is higher even at 3 GPa (~6 wt.%, Fig. 14), and is inferred to become significantly higher with increasing pressure. However, the composition of the near-solidus melts in the present study at $P > 3$ GPa is not $CaMgSi_2O_6$, but is more calcic. In order to understand how this shift in melt composition will affect the solubility of CO_2, we have to understand how CO_2 dissolves in CaO–MgO–SiO_2 melts.

Fine and Stolper (1986) proposed that CO_2 dissolved into diopside melt exclusively as carbonate, complexed with Ca and/or Mg. This solution mechanism has also been observed for other depolymerized melts (e.g., Fine and Stolper 1986; Brooker et al. 2001a, b). In contrast, CO_2 dissolves in more polymerized melts as both molecular CO_2 and carbonate (e.g., Fine and Stolper 1985; King and Holloway 2002), or (in the most polymerized) only as molecular CO_2 (Fogel and Rutherford 1990). If CO_2 dissolves in these melts as carbonate complexes, then the structural role of Ca and Mg will affect the relative stability of these complexes and hence the solubility of CO_2. Calcium is a network modifier,

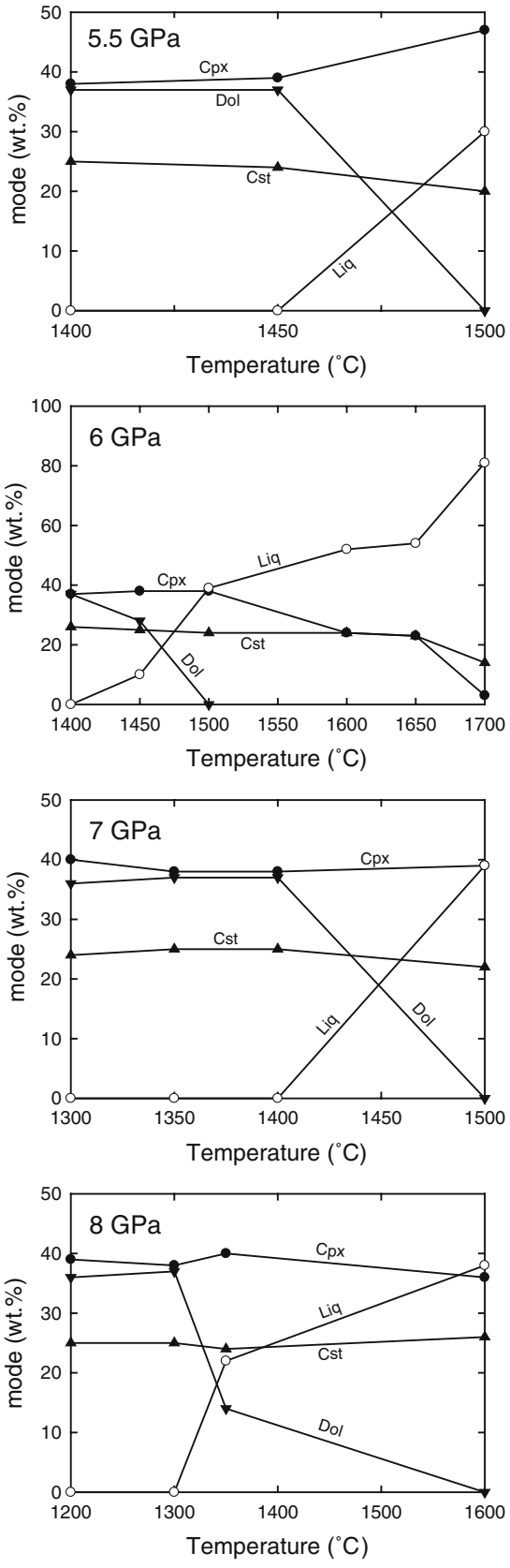

Fig. 15 Calculated modal abundances of phases present as a function of temperature at pressures at and above the intersection of the carbonation reaction with the solidus

Table 7 Melting reactions calculated from modes of sub- versus supersolidus experiments in the present study, normalized to 1 g liquid

P (GPa)	Reaction
5.5	1.23 Dol + 0.13 Cst = 1 Liq + 0.27 Cpx + 0.13 V
6	0.90 Dol + 0.10 Cst = 1 Liq + 0.10 Cpx
7	0.95 Dol + 0.08 Cst = 1 Liq + 0.03 Cpx
8	1.05 Dol + 0.05 Cst = 1 Liq + 0.09 Cpx

Abbreviations: As in Table 6, and *V* vapor

bonded to six oxygens, but Mg is surrounded by a more distorted arrangement of oxygens, with four oxygens being distinctly closer than an additional two (Angell et al. 1987; Matsui 1996; George and Stebbins 1998; Brooker et al. 2001a, b; Barbieri et al. 2004; Bonamartini Corradi et al. 2005). This difference has been taken to indicate that Mg plays a role more akin to a network former, at least for the purposes of understanding trends in CO_2 solubility (Brooker et al. 2001a, b), and these authors conclude that Mg is less reactive in terms of forming carbonate complexes compared to Ca.

Therefore, increasing Ca/Mg should increase CO_2 solubility, as has been observed at lower pressures by Holloway et al. (1976). The increasing Ca# in the melt as pressure increases from 3 to 5 GPa would increase CO_2 solubility, even if the pressure effect on solubility was absent. Thus the gradual decrease in solidus temperatures results from a more progressive evolution in melt composition from silicic to carbonatitic than in the lherzolite case. At higher pressures, the melt becomes dominated by such complexes, as is witnessed by the low silica content.

The change in modal abundances with increasing temperatures at $P \geq 5.5$ GPa clearly shows that liquid is produced primarily at the expense of carbonate, rather than clinopyroxene (Fig. 15). The modal abundances from the experiments that bracket the solidus at each pressure provide a basis to write melting reactions as a function of pressure (Table 7). These melting reactions verify the overwhelming contribution of carbonate to forming the melt, although the compositional change in the clinopyroxene across the solidus (Fig. 4) at 5.5 and 6 GPa requires that the clinopyroxene contribute Ca to the melt as well.

Comparison with carbonate melting

If carbonate is the dominant contributor to the melting reaction in this system, it is of interest to compare these results with those in the silicate-free $CaCO_3$–$MgCO_3$ system, particularly in light of recent suggestions that the melting relationships in this system strongly influence the solidus of carbonate-bearing eclogites (Yaxley and Brey 2004; Dasgupta et al. 2005). Buob (2003) and Buob et al. (2005) studied the $CaCO_3$–$MgCO_3$ join at 6 GPa. This study focused on the subsolidus phase relationships, but some supersolidus experiments were conducted to constrain the melting relationships (Fig. 16). Buob et al. comment on the ambiguities in the interpretation of the melting relationships because of

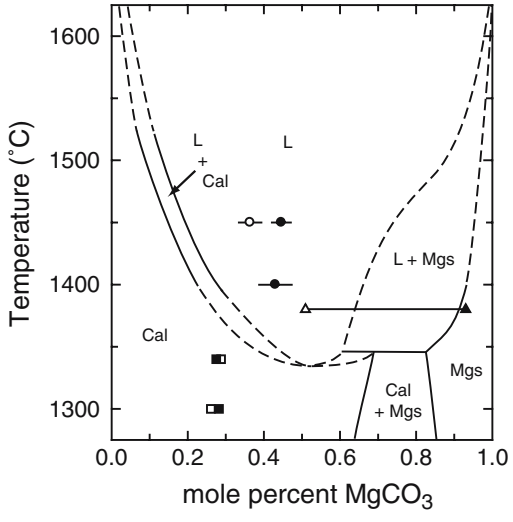

Fig. 16 Comparison of inferred phase relations for the $CaCO_3$–$MgCO_3$ system at 6 GPa (Buob et al. 2005) with the compositions of carbonates (*solid symbols*) and melts (*open symbols*) in more complex projected onto the binary. *Circles* 6 GPa carbonate and melt compositions in Di–CO_2 (this study). *Triangles* carbonate and melt coexisting with olivine, orthopyroxene, clinopyroxene, and garnet in the CaO–MgO–Al_2O_3–SiO_2–CO_2 system (Dalton and Presnall 1998). *Squares* coexisting carbonate and melt in carbonated eclogite at 5 GPa (Yaxley and Brey 2004). Phase relations for the $CaCO_3$–$MgCO_3$ binary shown as *dashed* where inferred by Buob et al.

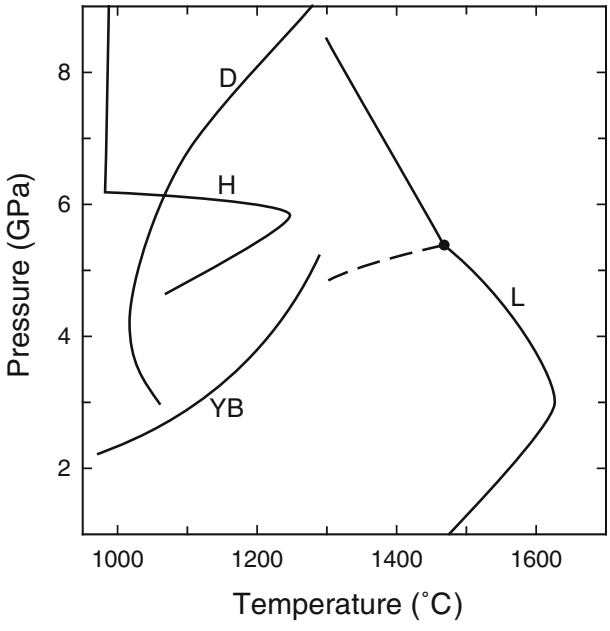

Fig. 17 Solidi for carbonate-bearing eclogites from three recent experimental studies compared to the solidus determined for the $CaMgSi_2O_6$–CO_2 system in the present study (L). *H* Hammouda (2003), *D* Dasgupta et al. (2004), *YB* Yaxley and Brey (2004)

Table 8 Melting reactions for carbonated eclogites, normalized to 1 g liquid

P (GPa)	Reaction
Hammouda (2003)	
5	4.13 Grt + 3.48 Cal + 3.09 Cst = 8.17 Cpx + 1.48 V + 1 Liq
6	1.51 Cal + 1.23 Grt + 0.41 Cst = 1.9 Cpx + 1 Liq + 0.23 V
6.5	0.97 Cal + 0.39 Grt + 0.27 Cst = 1 Liq + 0.63 Cpx
7	0.51 Arg + 0.49 Dol + 0.20 Grt = 1 Liq + 0.14 Cpx + 6 Cst
10	0.68 Arg + 0.35 Mgs + 0.26 Grt + 0.04 Cst = 1 Liq + 0.33 Cpx
Yaxley and Brey (2004)	
2.5	0.95 Carb + 0.19 Grt = 1 Liq + 0.14 Cpx
3	0.91 Carb + 0.10 Grt = 1 Liq + 0.02 Cpx
3.5	0.90 Carb + 0.20 Grt = 1 Liq + 0.10 Cpx
4.3	0.86 Carb + 0.08 Cpx + 0.06 Grt = 1 Liq
5.0	0.92 Carb + 0.11 Grt + 0.07 Cst = 1 Liq + 0.10 Cpx
Dasgupta et al. (2004)	
3	0.89 Carb + 0.33 Cpx = 1 Liq + 0.22 Grt + 0.11 Ilm
8.5	1.00 Mgs + 0.40 Cpx = 1 Liq + 0.40 Grt

Abbreviations: As in Table. 6 and 7, with additions of *Cal* calcite, *Arg* Aragonite, *Carb* carbonate

quench modification of these melts. Their data, combined with previous work at lower pressures (Byrnes and Wyllie 1981; Irving and Wyllie 1975), document a shift in the minimum melt in this system to progressively more magnesian compositions with increasing pressure, from Ca# = 67 at 1 GPa, 58 at 2.7 GPa to 49 at 6 GPa.

The composition of the melt at the solidus in the present study at 6 GPa has distinctly higher Ca# (64) compared with the minimum melt in the silicate-absent system (Fig. 16). Given that the Mg/Ca of the melt would be controlled by partitioning with clinopyroxene and carbonate, this difference is not surprising. This experiment contains a more magnesian carbonate (Ca# = 55) as a selvage at the bottom of the capsule (Table 1). If the melt and carbonate were in equilibrium, the partitioning of Ca and Mg are reversed from that predicted by binary phase relations. The melting phase relations inferred by Buob et al. (2005) have a minima on the solidus near Ca# = 50, so a melt more calcic than 50 should coexist with a carbonate that is even more calcic. Another puzzling difference is the minimum was constrained by Buob's experiments to be between 1,350 and 1,400°C. Melting in the present study was not detected until 1,450°C. Part of this difference may be explained by a carbonate composition different from that coexisting with the minimum melt. However, either small amounts of silicate suffice to change the phase relationships markedly from the carbonate endmember system, which seems implausible given the low silica content of melts (Table 4), or the near-solidus phase relationships in both systems merit further study. Given the difficulty in identifying near-solidus melts unambiguously in carbonate (and carbonate-bearing) systems (cf. discussions in Lee et al. 1994; Dalton and Presnall 1998; Yaxley and Brey 2004; Dasgupta et al. 2005), such a study may require a new experimental approach.

The correlation between phase relations in the $CaCO_3$–$MgCO_3$ system and silicate-bearing systems that is very good at 3 GPa (e.g., Fig. 3 of Dasgupta et al. 2005) seems to become more problematic at higher pressure based on other studies as well. The compositions of coexisting carbonate and melt in the CMAS–CO_2 study of Dalton and Presnall (1998) are consistent with the binary data in the sense that the Ca/Mg of the melt is greater than that of the coexisting carbonate, but the liquid is more calcic than expected from the binary phase relations (Fig. 16). The 5 GPa results of Yaxley and Brey (2004), also illustrated in Fig. 16, are difficult to reconcile with the melting relations in the $CaCO_3$–$MgCO_3$ system at either 3 or 6 GPa. The similarity in Ca/Mg of the melt and carbonate at both 1,300 and 1,340°C, and the reversal in Ca/Mg partitioning between melt and carbonate with increasing temperature, is not consistent with the form of the melting relationships in the binary at 3 or 6 GPa.

Comparison with carbonated eclogite solidi

There have been several recent studies of the melting behavior of carbonate-bearing eclogites (Hammouda 2003; Yaxley and Brey 2004; Dasgupta et al. 2004, 2005), using a variety of basaltic bulk compositions and a range of CO_2 contents. The location and overall shape of these solidi are quite variable, for reasons discussed by Yaxley and Brey (2004) and Dasgupta et al. (2004, 2005). Compared to the solidus determined in the present study (Fig. 17), all of the eclogite solidi are at lower temperatures, although that of Dasgupta et al. (2004) may approach the Di–CO_2 solidus at >8 GPa. This difference undoubtedly reflects the influence of additional constituents on the melting temperatures. The carbonate plays a major role in the melting reactions (Table 8), although to different extents depending on the bulk composition.

Conclusions

The temperature of the solidus in the $CaMgSi_2O_6$–CO_2 system decreases with increasing pressure from 3 to 8 GPa. This decrease is accompanied by a gradual change in the nature of the near-solidus melt from a silicate liquid with some dissolved CO_2 at 3 GPa to a

carbonatitic liquid with minimal SiO_2 by 5.5 GPa. In contrast to the peridotitic case, this evolution in melt composition is gradual and is not accompanied by an abrupt drop in solidus temperature at the pressure where the carbonation reaction intersects the solidus. This difference is explicable because of the higher pressure of this carbonation reaction relative to that for a lherzolite system, allowing the increasing solubility of CO_2 in the liquid with increasing pressure to produce a more gradual transition. In the Di-CO_2 system, as well as in the lherzolitic and eclogitic systems, once carbonate is a stable subsolidus phase, it plays a major role in the melting reaction at the solidus.

Acknowledgements This research was funded by a Discovery Grant from NSERC. In addition, the multi-anvil laboratory had been funded by a MFA grant from NSERC. The author acknowledges with thanks the assistance of Diane Caird in the high-pressure laboratory and the assistance of Sergei Matveev with the electron microprobe. Constructive reviews by Greg Yaxley and Rajdeep Dasgupta of an earlier version of this manuscript were very helpful.

References

Angell CA, Cheesman PA, Kadiyala RR (1987) Diffusivity and thermodynamic properties of diopside and jadeite melts by computer simulation studies. Chem Geol 62:83–92

Barbieri L, Bonamartini Corradi A, Lancellotti I, Leonelli C, Montorsi M (2004) Experimental and computer simulation study of glasses belonging to diopside-anorthite system. J Non Cryst Sol 345–346:724–729

Boettcher AL, Burnham CW, Windom KE, Bohlen SR (1982) Liquids, glasses, and the melting of silicates to high pressures. J Geol 90:127–138

Bohlen SR (1984) Equilibria for precise pressure calibration and a frictionless furnace assembly for the piston-cylinder apparatus. Neus Jahrb Mineral Monatsh H 9:404–412

Bonamartini Corradi A, Bondioli F, Cannillo V, Ferrari AM, Lancellotti I, Montorsi M (2005) The anorthite-diopside system: structural and devitrification study. Part I: structural characterization by molecular dynamic simulations. J Am Ceram Soc 88:714–718

Brey GP, Green DH (1976) Solubility of CO_2 in olivine melilitite at high pressures and role of CO_2 in the Earth's upper mantle. Contrib Mineral Petrol 55:217–230

Brooker RA, Kohn SC, Holloway JR, McMillan PF (2001a) Structural controls on the solubility of CO_2 in silicate melts. Part I: bulk solubility data. Chem Geol 174:225–239

Brooker RA, Kohn SC, Holloway JR, McMillan PF (2001b) Structural controls on the solubility of CO_2 in silicate melts. Part II: IR characteristics of carbonate groups in silicate glasses. Chem Geol 174:241–254

Buob A (2003) The system $CaCO_3$–$MgCO_3$: experiments and thermodynamic modeling of the trigonal and orthorhombic solid solutions at high pressure and temperature. Dr. Nat. Sci. Thesis, Swiss Federal Institute of Technology (unpublished)

Buob A, Luth RW, Schmidt MW, Ulmer P (2005) Experiments on $CaCO_3$–$MgCO_3$ solid solutions at high pressure and temperature. Am Mineral (in press)

Byrnes AP, Wyllie PJ (1981) Subsolidus and melting relations for the join $CaCO_3$–$MgCO_3$ at 10 kbars. Geochim Cosmochim Acta 45:321–328

Carr MJ (2002) IGPET for Windows. Version June 12, 2002. Terra Softa Inc., 155 Emerson Road, Somerset N.J. 08873 U.S.A

Dalton JA, Presnall DC (1998) Carbonatitic melts along the solidus of model lherzolite in the system CaO–MgO–Al_2O_3–SiO_2–CO_2 from 3 to 7 GPa. Contrib Mineral Petrol 131:123–135

Dalton JA, Wood BJ (1993) The compositions of primary carbonate melts and their evolution through wallrock reaction in the mantle. Earth Planet Sci Lett 119:511–525

Dasgupta R, Hirschmann MM, Withers AC (2004) Deep global cycling of carbon constrained by the solidus of anhydrous, carbonated eclogite under upper mantle conditions. Earth Planet Sci Lett 227:73–85. DOI 10.1016/j.epsl.2004.08.004

Dasgupta R, Hirschmann MM, Dellas N (2005) The effect of bulk composition on the solidus of carbonated eclogite from partial melting experiments at 3 GPa. Contrib Mineral Petrol 149:288–305. DOI 10.1007/s00410-004-0649-0

Domanik KJ, Luth RW (1999) The effect of pressure on thermal gradients in multianvil apparatus. EOS 80:S335

Eggler DH (1974) Effect of CO_2 on the melting of peridotite. Carnegie Inst Wash Year Bk 73:215–224

Eggler DH (1976) Does CO_2 cause partial melting in the low-velocity layer of the mantle? Geology 4:69–72

Eggler DH (1978) The effect of CO_2 upon partial melting of peridotite in the system Na_2O–CaO–Al_2O_3–MgO–SiO_2–CO_2 to 35 kb, with an analysis of melting in a peridotite–H_2O–CO_2 system. Am J Sci 278:305–343

Eggler DH, Rosenhauer M (1978) Carbon dioxide in silicate melts: II. Solubilities of CO_2 and H_2O in $CaMgSi_2O_6$ (diopside) liquids and vapors at pressures to 40 kb. Am J Sci 278:64–94

Fine G, Stolper E (1985) The speciation of carbon dioxide in sodium aluminosilicate glasses. Contrib Mineral Petrol 91:105–121

Fine G, Stolper E (1986) Dissolved carbon dioxide in basaltic glasses: concentration and speciation. Earth Planet Sci Lett 76:263–278

Fogel RA, Rutherford MJ (1990) The solubility of carbon dioxide in rhyolitic melts: a quantitative FTIR study. Am Mineral 75:1311–1326

George AM, Stebbins JF (1998) Structure and dynamics of magnesium in silicate melts: a high-temperature ^{25}Mg NMR study. Am Mineral 83:1022–1029

Gudfinnsson GH, Presnall DC (2005) Continuous gradations among primary carbonatitic, kimberlitic, melilititic, basaltic, picritic, and komatiitic melts in equilibrium with garnet lherzolite at 3–8 GPa. J Petrol. DOI 10.1093/petrology/egi029

Hammouda T (2003) High-pressure melting of carbonated eclogite and experimental constraints on carbon cycling and storage in the mantle. Earth Planet Sci Lett 214:357–368. DOI 10.1016/S0012-812X(03)00361-3

Hirose K (1997) Partial melt compositions of carbonated peridotite at 3 GPa and role of CO_2 in alkali-basalt generation. Geophys Res Lett 24:2837–2840

Holloway JR, Blank JG (1994) Application of experimental results to C–O–H species in natural melts. In: Carroll MR, Holloway JR (eds) Volatiles in magmas, Chapter 6. Review in Mineral vol 30. Mineral Society of America, Washington DC

Holloway JR, Mysen BO, Eggler DH (1976) The solubility of CO_2 in liquids on the join CaO–MgO–SiO_2–CO_2. Carnegie Inst Wash Year Book 75:626–630

Irving AJ, Wyllie PJ (1975) Subsolidus and melting relationships for calcite, magnesite and the join $CaCO_3$–$MgCO_3$ to 36 kbar. Geochim Cosmochim Acta 39:35–53

King PL, Holloway JR (2002) CO_2 solubility and speciation in intermediate (andesitic) melts: the role of H_2O and composition. Geochim Cosmochim Acta 66:1627–1640

Knoche R, Sweeney RJ, Luth RW (1999) Carbonation and decarbonation of eclogites: the role of garnet. Contrib Mineral Petrol 135:332–339

Lee W-J, Wyllie PJ, Rossman GR (1994) CO_2-rich glass, round calcite crystals, and no liquid immiscibility in the system CaO–SiO_2–CO_2 at 2.5 GPa. Am Mineral 79:1135–1144

Luth RW (1995) Experimental determination of the reaction dolomite + 2 coesite = diopside + 2 CO_2 to 6 GPa. Contrib Mineral Petrol 122:152–158

Luth RW (1999) Carbon and carbonates in the mantle. In: Fei Y, Bertka CM, Mysen BO (eds) Mantle petrology: field observations and high pressure experimentation: a tribute to Francis R. (Joe) Boyd. Geochem Soc Spec Pub No 6, pp 297–316

Luth RW (2001) Experimental determination of the reaction aragonite + magnesite = dolomite at 5 to 9 GPa. Contrib Mineral Petrol 141:222–232

Matsui M (1996) Molecular dynamics simulation of structures, bulk moduli, and volume thermal expansivities of silicate liquids in the system $CaO–MgO–Al_2O_3–SiO_2$. Geophys Res Lett 23:395–398

Moore KR, Wood BJ (1998) The transition from carbonate to silicate melts in the $CaO–MgO–SiO_2–CO_2$ system. J Petrol 39:1943–1951

Mysen BO, Eggler DH, Seitz MG, Holloway JR (1976) Carbon dioxide in silicate melts and crystals. I. Solubility measurements. Am J Sci 276:455–479

Rai CS, Sharma SK, Muenow DW, Matson DW, Byers CD (1983) Temperature dependence of CO_2 solubility in high pressure quenched glasses of diopside composition. Geochim Cosmochim Acta 47:953–958

Schmidt MW, Ulmer P (2004) A rocking multianvil: elimination of chemical segregation in fluid-saturated high-pressure experiments. Geochim Cosmochim Acta 68:1889–1899. DOI 10.1016/j.gca.2003.10.031

Shirasaka M, Takahashi E, Nishihara Y, Matsukage K, Kikegawa T (2002) In situ X-ray observation of the reaction dolomite = aragonite + magnesite at 900–1300 K. Am Mineral 87:922–930

Stalder R, Ulmer P (2001) Phase relations of a serpentine composition between 5 and 14 GPa: significance of clinohumite and phase E as water carriers into the transition zone. Contrib Mineral Petrol 140:670–679. DOI 10.1007/s004100000208. Also cf. erratum in Contrib Mineral Petrol 140:754. DOI 10.1007/s004100100246

Susaki J, Akaogi M, Akimoto S, Shimomura O (1985) Garnet-perovskite transformation in $CaGeO_3$: in-situ x-ray measurements using synchrotron radiation. Geophys Res Lett 12:729–732

Sweeney RJ (1994) Carbonatite melt compositions in the Earth's mantle. Earth Planet Sci Lett 128:259–270

Wallace ME, Green DH (1988) An experimental determination of primary carbonatite magma composition. Nature 335:343–346

Walter MJ (1998) Melting of garnet peridotite and the origin of komatiite and depleted lithosphere. J Petrol 39:29–60

Walter MJ, Thibault Y, Wei K, Luth RW (1995) Characterizing experimental pressure and temperature conditions in multi-anvil apparatus. Can J Phys 73:273–286

White BS, Wyllie PJ (1992) Solidus reactions in synthetic lherzolite–$H_2O–CO_2$ from 20–30 kbar, with applications to melting and metasomatism. J Volcanol Geotherm Res 50:117–130

Williams DW, Kennedy GC (1969) Melting curve of diopside to 50 kilobars. J Geophys Res 74:4359–4366

Wyllie PJ, Huang WL (1975) Peridotite, kimberlite, and carbonatite explained in the system $CaO–MgO–SiO_2–CO_2$. Geology 3:621–624

Wyllie PJ, Huang WL (1976) Carbonation and melting reactions in the system $CaO–MgO–SiO_2–CO_2$ at mantle pressures with geophysical and petrological applications. Contrib Mineral Petrol 54:79–107

Yagi T, Akimoto S (1976) Direct determination of coesite-stishovite transition by in-situ X-ray measurements. Tectonophysics 35:259–270

Yaxley GM, Brey GP (2004) Phase relations of carbonate-bearing eclogite assemblages from 2.5 to 5.5 GPa: implications for petrogenesis of carbonatites. Contrib Mineral Petrol 146:606–619. DOI 10.1007/s00410-003-0517-3